Thermodynamic analysis of III–V semiconductor alloys grown by metalorganic vapor phase epitaxy

Toshihiro Asai and David S. Dandy[a)]
Department of Chemical Engineering, Colorado State University, Fort Collins, Colorado 80523-1370

(Received 22 February 2000; accepted for publication 7 July 2000)

A thermodynamic analysis has been applied to systematically study III–V semiconductor alloy deposition, including nitrides grown by metalorganic vapor phase epitaxy. The predicted solid compositions of a number of ternary and quaternary alloys, including $Al_xGa_{1-x}P_yAs_{1-y}$, are compared with experimental data. For phosphorus-containing alloys, introduction of a parameter f representing incomplete PH_3 pyrolysis yields good agreement with experimental data. It is shown that the input mole fraction of the group III metalorganic sources influences the incorporation of P into the solid for these alloys. Solid composition is also calculated for nitride alloys as a function of inlet gas concentration. To date, thermodynamic models have been applied solely to predict N solubility limits for nitride alloys where mixing occurs on the group V sublattice. The present model is used to predict N solid compositions in ternary and quaternary alloys, and it is demonstrated that these values are below the theoretical solubility limits for In-containing nitrides. The role of H_2 in the carrier gas is investigated for III–N–V, III–III–N–V, and III–N–V–V systems. © *2000 American Institute of Physics.* [S0021-8979(00)03520-9]

I. INTRODUCTION

Stringfellow and co-workers[1–5] first proposed a model to predict the solid composition of III–V alloys deposited via metalorganic chemical vapor phase epitaxy (MOVPE) whereby it was assumed that thermodynamic equilibrium was established at the solid–gas interface. Accurate prediction of Sb composition in the solid phase for $GaAs_{1-y}Sb_y$ and $InAs_{1-y}Sb_y$ was found to be possible using this approach. However, for phosphorus-containing alloys, this model cannot be directly applied, and a kinetic factor related to incomplete pyrolysis of the PH_3 precursor must be included. To address this issue, Stringfellow *et al.*[6] investigated the alloys $GaP_{1-y}Sb_y$ and $InP_{1-y}Sb_y$. By relating known Sb solid compositions to inlet gas-phase Sb concentrations, an adjustable parameter, K_{int}, representing the extent of pyrolysis of PH_3 could be calculated.

Using this approach, Koukitu *et al.*[7,8] computed the solid compositions of many useful III–V semiconductor alloys, including P-containing alloys. They included a constraint in their model that the equilibrium partial pressures for major species must sum to the total pressure of the system. They also incorporated group V dimer species into Stringfellow's models.[1–5] Very good agreement between predicted solid compositions and experimental data were obtained for GaP_yAs_{1-y}, InP_yAs_{1-y} and $InP_xAs_ySb_{1-x-y}$.

In the present work, the alloys containing different group III (Al, Ga, and In) and group V (N, P, As, and Sb) elements are systematically studied using a model similar to the one developed by Koukitu *et al.*[7,8] A total of 30 III–III–V and III–V–V ternary alloys, plus another 30 III–III–III–V, III–III–V–V, and III–V–V–V quaternary alloys are modeled. However, the primary focus of this work is to predict the solid composition of nitrogen in III–V nitride alloys, which have been identified as promising optoelectronic materials.[9–11] Among the broad class of optoelectronic materials, vertical-cavity surface emitting lasers (VCSELs) have recently been given close attention because of their promise for use in a wide range of applications.[12] MOVPE has advantages for VCSEL growth over other epitaxial techniques, including molecular beam epitaxy (MBE) and chemical beam epitaxy (CBE). In principle, MOVPE is capable of producing an interface free of barriers through the use of a continuously graded profile.[13] Unfortunately, most of the thermodynamic analysis thus far on nitrides has examined mixing on the group III sublattice.[14–17] Studies on nitrides with mixing on the group V sublattice are scarce and limited to the calculation of solubility limits.[18,19] This is due in part to the large miscibility gaps expected for these alloys, but is also due to the necessity of including a kinetic factor related to incomplete NH_3 decomposition.

Therefore, as a first step, it is shown here that a general thermodynamic model can be applied to a simpler kinetically controlled system, the InP_yAs_{1-y} alloy. Thermodynamic analysis for the quaternary $Al_xGa_{1-x}P_yAs_{1-y}$ alloy is also presented in detail. Then, the model is applied to predict the solid composition of nitrogen in the more complicated III–V nitride system, which is another kinetically controlled system. The N solid compositions of various III–V nitrides with mixing on the group V sublattice, that is, InN_yAs_{1-y}, AlN_yAs_{1-y}, $Al_xGa_{1-x}N_yAs_{1-y}$, $Al_xIn_{1-x}N_yAs_{1-y}$, $Ga_xIn_{1-x}N_yAs_{1-y}$, $AlN_xP_yAs_{1-x-y}$, and $AlN_xP_ySb_{1-x-y}$ are investigated. Also, N solid composition in $Ga_xIn_{1-x}N$ is presented to illustrate the difference between the present model and Koukitu's.[17] It is demonstrated that, in principle, the thermodynamic analysis of any ternary or quaternary III–V alloy is possible using this model and approach.

a)Electronic mail: david.dandy@colostate.edu

II. MODEL AND CALCULATION PROCEDURE

A. General model

The model previously proposed by Koukitu *et al.*[7,8] is used to calculate solid composition and equilibrium gas partial pressure for III–V alloys. However, a modification of Koukitu's model is made to include the kinetically controlled factor, K_{int}, describing the degree of dissociation of the group V source molecules. To calculate thermodynamic properties such as solid composition and equilibrium partial pressure, it is necessary to solve a set of simultaneous nonlinear algebraic equations subject to the following assumptions: (1) the pyrolysis of group III and group V source molecules is complete, with the exceptions of PH_3 and NH_3; and (2) thermodynamic equilibrium is established near the solid–gas interface. The model will be applied to the growth of a $A^{\text{III}}B_y^{\text{V}}C_{1-y}^{\text{V}}$ ternary alloy using trimethylaluminum (TMAl), trimethylgallium (TMGa), trimethylindium (TMIn), phosphine (PH_3), or arsine (AsH_3) as the sources. Complete pyrolysis of all group III precursors is assumed in this work because only trimethyl alkyl species have been considered. The deposition reaction occurring near the solid–gas interface is

$$\text{III}(g)+\tfrac{1}{4}\text{V}_4(g)\Leftrightarrow \text{III}-\text{V}(s), \tag{1}$$

where III and V denote the group III and the group V elements. Since it is known that PH_3 does not, in general, completely pyrolyze, it is possible that the group III element may react directly with PH_3 in addition its tetramer decomposition product, P_4. However, the stability of PH_3 relative to P_4 provides Eq. (1) with a much stronger driving force.

At equilibrium, the mass action expression associated with this reaction is

$$K_{\text{III-V}}=\frac{a_{\text{III-V}}}{P_{\text{III}}P_{\text{V}_4}^{1/4}}, \tag{2}$$

where $a_{\text{III-V}}$ denotes the activity of the III–V alloy, P_{III} is the equilibrium partial pressure of the group III atom in the gas phase, and P_{V_4} is the equilibrium partial pressure of the group V tetramer molecule. Assuming ideal gas law behavior, the total pressure P of the system, assumed known, is written as

$$P=\sum P_{\text{i}}=P_{\text{III}}+P_{\text{V}_4}+P_{\text{V}_2}+P_{\text{V}}+P_{\text{H}_2}+P_{\text{CH}_4}, \tag{3}$$

where P_{V_2} and P_{V} are the equilibrium partial pressures of the group V dimer molecules and the group V source molecules, respectively. The equilibrium partial pressures of H_2 and CH_4 are included in Eq. (3) because these species are produced by the pyrolysis of the group III and group V source molecules and H_2 may be present as a carrier gas. The conservation constraint on the stoichiometry of the deposited solid requires that the total moles of the group III elements be equal to the moles of the group V elements in the solid

$$P_{\text{III}}^0-P_{\text{III}}=P_{\text{V}}^0-4P_{\text{V}_4}-2P_{\text{V}_2}-P_{\text{V}}, \tag{4}$$

where P_{III}^0 and P_{V}^0 are the inlet partial pressures of the group III and group V species. The conservation constraint on solid composition requires that the solid fraction of group III elements and that of group V elements be unity:

$$y=\frac{P_{\text{V}}^0-4P_{\text{V}_4}-2P_{\text{V}_2}-P_{\text{V}}}{(P_{\text{V}}^0-4P_{\text{V}_4}-2P_{\text{V}_2}-P_{\text{V}})+(P_{\text{V}}^0-4P_{\text{V}_4'}-2P_{\text{V}_2'}-P_{V'})}. \tag{5}$$

Activities of component III–V binary compounds are determined using the delta lattice parameter (DLP) model.[18] The value of the proportionality factor K in the DLP model is taken to be 1.15×10^7 cal Å/mole for non-nitrides and 1.07×10^7 cal Å/mole for nitrides. The solid composition and equilibrium partial pressures of all gas species are calculated using an Argonne National Laboratory code, Hybrid Method, which was developed to solve highly nonlinear systems of equations. The code is a modified Newton's scheme, with approximate Jacobian evaluation. The equilibrium constants for the reactions are evaluated as $\exp(-\Delta G_f/RT)$, where G_f is the Gibbs free energy of formation, R is the gas constant, and T is the growth temperature. The Gibbs energies associated with GaN, InN, and AlN deposition are obtained from the literature.[16] However, the equilibrium constants associated with AlP and AlAs deposition which are experimentally determined by Koukitu *et al.*[20,21] are used because the Gibbs free energies of these alloys are not available. Unless otherwise indicated, the equilibrium constants calculated via $\exp(-\Delta G_f/RT)$ are used in the model predictions. The values of Gibbs free energy were extracted from the data of Pankratz.[22]

B. Kinetic factors

Two different parameters are introduced to represent the effects of incomplete $PH_3$and NH_3 pyrolysis. It is known that the pyrolysis rates of $PH_3$and NH_3 are slow relative to typical reactor resistance times. However, there are important distinctions between these two reactant species. In practice there are two principal products of PH_3 decomposition, P_4 and P_2, which coexist with one another in equilibrium; and the extent of PH_3 decomposition may be determined using one adjustable parameter, f, combined with the P_4/P_2 equilibrium constant. For nitrides, however, there is only one nitrogen-containing product of NH_3 decomposition, N_2. In lieu of using the equilibrium constant related to NH_3 decomposition, an adjustable parameter α is introduced to represent the extent of NH_3 decomposition. Furthermore, the tetramer, P_4, and dimer, P_2, are the precursors involved in the deposition of phosphides, while the inlet species PH_3 does not directly participate in the deposition process. Thus, it is desirable to enhance PH_3 decomposition as much as possible. In nitride systems, NH_3 is directly involved in the deposition process, while the dimer N_2 is effectively inert. Thus, in contrast with phosphides, it is desirable to minimize NH_3 decomposition.

The equilibrium expression for PH_3 pyrolysis is

$$K_{\text{eq}}=\frac{P_{\text{P}_2}^{1/2}P_{\text{H}_2}^{3/2}}{P_{\text{PH}_3}}. \tag{6}$$

The reaction described in Eq. (6) will not, in general, apply, since PH_3 decomposition will not reach equilibrium. Using a fitting parameter f, the extent of PH_3 pyrolysis may be expressed as

$$K_p = fK_{eq} \quad (f \leqslant 1), \tag{7}$$

with a maximum value equal to the equilibrium constant K_{eq} when $f=1$. The quantity K_p is equivalent to the parameter K_{int} in Stringfellow's model.[6] The parameter f depends on quantities such as growth temperature, deposition area, species' partial pressures, the possible presence of a catalyst, total flow rate, and reactor geometry.

Instead of applying the parameter f described above to quantify NH_3 decomposition, the parameter α used in Koukitu's model is applied.[17] The sole reason for this approach is to distinguish between PH_3 and NH_3 pyrolysis. The decomposition of NH_3, which occurs near the solid–gas interface, may be written as

$$NH_3(g) \rightarrow (1-\alpha)NH_3(g) + \tfrac{1}{2}\alpha N_2(g) + \tfrac{3}{2}\alpha H_2(g), \tag{8}$$

where α is the mole fraction of NH_3 decomposing. Unlike Koukitu's model,[17] the partial pressure of N_2 is included in the mass conservation constraint, an expression analogous to Eq. (4); furthermore, the parameter α appears in the stoichiometry and solid composition conservation constraints.

C. Modeling nitride growth

In contrast with other group V materials, the presence of H_2 in the system affects the deposition of nitrides, and the analysis of these III–V alloys must be modified to include this effect. The dependence of nitride growth on H_2 concentration may be explained by Le Chatelier's principle. During growth of more conventional III–V alloys such as GaP, hydrogen is not produced during the deposition process, as illustrated by the reversible reaction, Eq. (1), applied to GaP:

$$Ga(g) + \tfrac{1}{4}P_4 \Leftrightarrow GaP(s). \tag{9}$$

On the other hand, deposition of III–V nitrides such as GaN does result in hydrogen production, as shown for GaN deposition:

$$Ga(g) + NH_3(g) \Leftrightarrow GaN(s) + \tfrac{3}{2}H_2(g). \tag{10}$$

The excess H_2 produced in the system will perturb the equilibrium state and the reaction in Eq. (10) will shift towards the left hand side to reestablish a new equilibrium state. Hence, the deposition of III–V nitrides benefits from the presence of an inert carrier gas. Also, the extent of NH_3 decomposition should be small to suppress the amount of H_2 in the system. Because of the presence of an additional component, the inert carrier, a parameter F, representing the mole fraction of H_2 in the carrier gas, is introduced, such that $F = P^0_{H_2}/(P^0_{H_2} + P^0_{IG})$, where $P^0_{H_2}$ and P^0_{IG} denote the inlet partial pressures of H_2 and inert gas, respectively.

In practice, the growth of nitride alloys can be difficult, particularly those alloys with mixing on the group V sublattice. This is due to the large miscibility gaps expected for these alloys. As a result, the theoretical values for N solid fraction are also very low compared with the solid fraction of conventional group V elements such as P and As. For example, in the present work the predicted N solid fraction in InN_yAs_{1-y} is approximately 1.0×10^{-5} for temperatures ranging from 550 to 650 °C. It is, therefore, desirable to compare the calculated results of N solid fractions with theoretical values for N solubility limits. If both theoretical approaches are sound the predicted N solid fraction in an alloy should be lower than the predicted N solubility limit. The theoretical solubility limit of N in the solid, x, may be calculated using the expression[18]

$$x = \exp(-\Omega/RT), \tag{11}$$

where Ω is the interaction parameter, R is the ideal gas constant, and T is the growth temperature. Ho and Stringfellow[23] computed the interaction parameters for several III–V nitrides using the valence force field (VFF) model,[24] which calculates the strain energy due to stretching and bending of bonds. However, Schilfgaarde *et al.*[25] pointed out that the VFF model is not appropriate for calculating N solubility limit for alloys such as $Al_{1-x}Ga_xN$, where the strain energy does not dominate the enthalpy of mixing, H.

III. RESULTS AND DISCUSSION

Thermodynamic calculations described above are carried out for 60 ternary and quaternary alloys, but only a representative subset of these: InP_yAs_{1-y}, $Al_xGa_{1-x}P_yAs_{1-y}$, $Ga_{1-x}In_xN$, InN_yAs_{1-y}, AlN_yAs_{1-y}, $Al_xGa_{1x}N_yAs_{1-y}$, $Al_xIn_{1-x}N_yAs_{1-y}$, $Ga_xIn_{1-x}N_yAs_{1-y}$, $AlN_xP_yAs_{1-x-y}$, and $AlN_xP_ySb_{1-x-y}$ are presented here.

A. Non-nitrides

The inlet group III partial pressure of 5×10^{-5} atm used by Koukitu *et al.*[7,8] is applied to the prediction of solid compositions for these materials. This value is consistent with the group III vapor pressures found at typical bubbler temperatures.[26] The parameter f, that is, the extent of PH_3 pyrolysis, is much smaller than unity in the normal range of growth temperatures used for arsenide–phosphide alloys, from 550 to 700 °C.[27,28] Growth temperatures of 650 and 700 °C are used in the present calculations.

1. Ternary III–V–V alloys

InP_yAs_{1-y}: Solid compositions of InP_yAs_{1-y} have been computed as a function of inlet phosphorus fraction, for inlet V/III ratios ranging from 1 to 200. Figure 1 shows the prediction for a single inlet ratio $V^0/III^0 = 180$, at a processing temperature of 600 °C, together with experimental data taken under the same conditions.[29] In that calculation the degree of PH_3 decomposition was chosen to be $f=0.007$, indicating that the decomposition of this species reached less than 1% of the equilibrium state. The preferential incorporation of As over P can be seen in Fig. 1, even though the Gibbs free energy of formation for binary compounds predicts the preferential incorporation of P over As, that is, $K_{InP} > K_{InAs}$. This behavior is predicted for all values of V^0/III^0 considered, and it becomes more pronounced as V^0/III^0 increases. The good agreement between theoretical prediction and the experimental data suggest that the Gibbs free energy of formation of binary compounds alone cannot predict the preferred

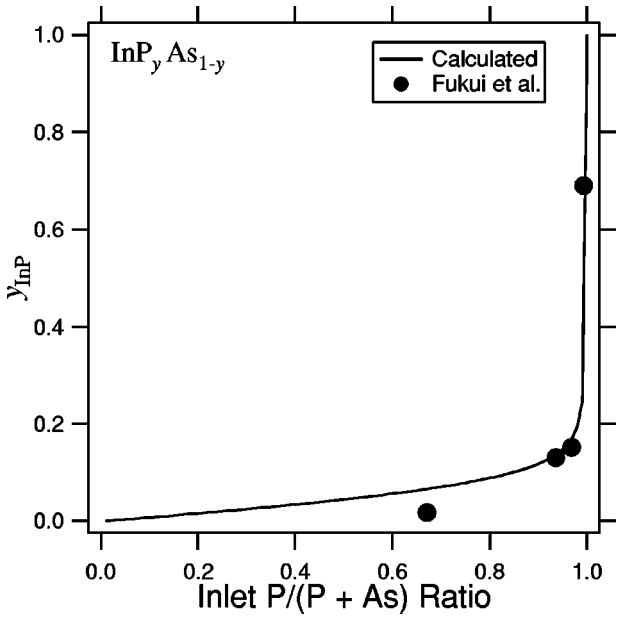

FIG. 1. Solid vs gas composition for the alloy InP_yAs_{1-y}, for $P^0_{In}=1.0\times10^{-5}$ atm, temperature 600 °C, and $V^0/III^0=180$, accounting for incomplete pyrolysis of PH_3 ($f=0.007$). The experimental data are from Ref. 29.

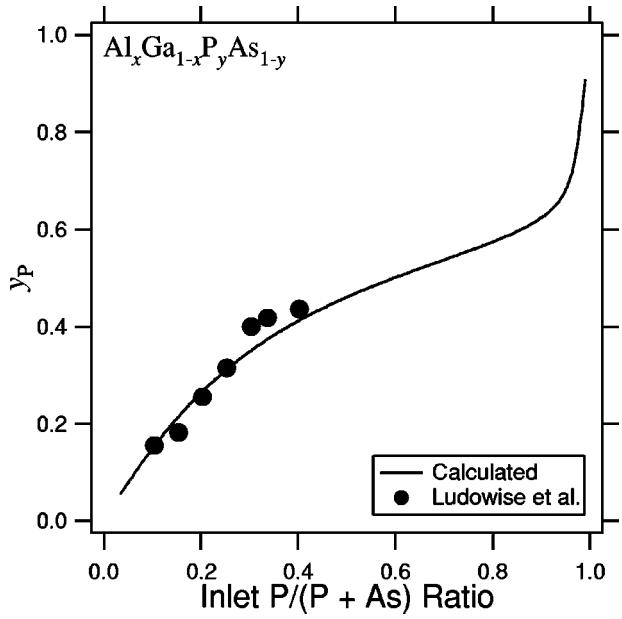

FIG. 2. Solid vs gas composition for the alloy $Al_xGa_{1-x}P_yAs_{1-y}$, for $P^0_{III}=1.0\times10^{-5}$ atm, growth temperature of 750 °C, $V^0/III^0=10$, and $P^0_{TMAl}/P^0_{III}=0.6$, considering incomplete pyrolysis of PH_3 ($f=0.12$). The equilibrium constants related to AlP and AlAs deposition are from Refs. 20 and 21. The experimental data are from Ref. 30.

incorporation of elements into the solid phase. It also indicates that the kinetically controlled factor related to incomplete pyrolysis of PH_3 plays an important role in determining solid composition in this system.

2. Quaternary III–III–V–V alloys

$Al_xGa_{1-x}P_yAs_{1-y}$: For the $Al_xGa_{1-x}P_yAs_{1-y}$ alloy it is predicted that the solid fraction of Al increases linearly with inlet TMAl gas concentration over the entire range of $P^0_{PH_3}/P^0_V$ ratios considered. This linear relationship for solid–gas composition holds for the range of growth temperatures (650–800 °C) and V^0/III^0 ratios (>1) characteristic of normal growth conditions, and correlates well with experimental observation.[30] Although the fraction of Al in the solid increases linearly with inlet TMAl concentration, this quantity is almost independent of the V^0/III^0 concentration ratio. The fraction of P in the solid phase increases nonlinearly with increasing inlet PH_3 gas concentration, and this fraction also increases with increasing P^0_{TMAl}/P^0_{III} ratio, once again correlating well with experimental observation.[30] The observation that the group V solid fraction depends on the III gas concentration while the group III solid fraction is independent of the group V gas concentration is explained by the fact that III–V semiconductors grown by MOVPE are mass transport limited in the group III molecules. Consequently, particularly for the quaternary alloys, precise control of gas-phase composition is essential for control of solid-phase composition. In Fig. 2, the predicted values of the phosphorus fraction in the $Al_xGa_{1-x}P_yAs_{1-y}$ alloy for a growth temperature of 750 °C are compared with experimental data.[30] Incomplete PH_3 pyrolysis was accounted for in these calculations; the values of the equilibrium constants associated with AlP and AlAs deposition are taken from Koukitu *et al.*[20,21]

B. Nitrides

Ternary nitrogen-containing alloys, $Ga_xIn_{1-x}N$ for example, are typically grown at temperatures ranging between 650 and 800 °C;[31] for this particular ternary alloy the optimal growth temperature has been determined to be 700 °C.[32] To this end, growth temperatures of 700 and 800 °C are used for the prediction of N solid composition in the ternary nitride alloys considered here. For these calculations, an inlet group III partial pressure of 1.0×10^{-5} atm is assumed. Less data are available for quaternary nitride alloys, but lattice matched $Ga_xIn_{1-x}N_yAs_{1-y}$ has been grown by Kurtz *et al.*,[33] and the optimized growth temperature was found to be 650 °C for an annealing time of 30 min, or 700 °C for an annealing time of 2 min. Thus, growth temperatures of 600 and 700 °C are used for the prediction of N solid composition in quaternary nitride alloys. The value of the NH_3 decomposition parameter α is varied for III–III–N alloys to investigate the difference between the present model and that of Koukitu *et al.*[17] However, except for the III–III–N alloy, α is set to zero for simplicity and only F is varied because the effect of changing α can be incorporated in F. In other words, for the purposes of the calculations the H_2 produced by NH_3 decomposition can be accounted for by altering the H_2 initially present in the carrier gas.

1. Ternary III–III–N alloys

$Ga_xIn_{1-x}N$: The dependence of the solid composition of $Ga_{1-x}In_xN$ on the fractional decomposition of NH_3 has been calculated. The solid fraction of In increases linearly with increasing P^0_{TMIn} when $\alpha=0$ (no NH_3 decomposition), but for $\alpha>0.2$, the relationship between solid and gas composition deviates from a linear function, and the fraction of In in the solid decreases significantly. This deviation from linear

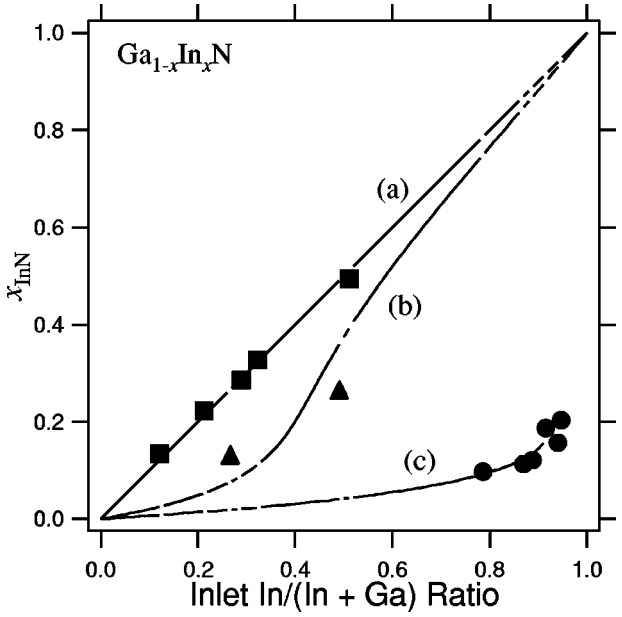

FIG. 3. Solid vs gas composition for the alloy $Ga_{1-x}In_xN$, for temperatures of 500, 700, and 800 °C. The conditions were the same as those used by Ref. 34, that is, (a) $P^0_{III}=3.6\times10^{-6}$ atm, $V^0/III^0=20\,000$, mole fraction of NH_3 decomposing $\alpha=0.1$; (b) $P^0_{III}=3.6\times10^{-6}$ atm, $V^0/III^0=25\,000$, $\alpha=0.72$; (c) $P^0_{III}=1.0\times10^{-5}$ atm, $V^0/III^0=5000$, $\alpha=0.62$. The solid lines represent the present calculations while the symbols denote experimental measurements.

behavior occurs at a higher value of α than predicted by Koukitu *et al.*[17] For example, for $P^0_{TMIn}/P^0_{III}=0.7$ the In solid fraction is predicted by the Koukitu *et al.* model to be approximately 0.1 when $\alpha=0.2$, while $x_{InN}\approx0.1$ at $\alpha=0.5$ in the present study. This disparity suggests that the earlier model overestimates the effect of NH_3 decomposition on the deviation of In solid fraction from a linear function. This difference between the two calculations arises because the present model includes the effect of N_2 produced by NH_3 decomposition in the constraint on total system pressure and in the solid-phase mass conservation constraints. In Fig. 3, the predicted In solid fractions are compared with the experimental data of Matsuoka *et al.*[34] For this comparison the calculations have been carried out using α as a fitting parameter. The agreement between the theoretical predictions and experimental data is quite good, which shows that a quasithermodynamic equilibrium model is valid for this system. Again, the values of α used in this calculation are larger than those used by Koukitu *et al.*[17]

2. Ternary III–N–V alloy

InN_yAs_{1-y}: Figures 4 and 5 show the theoretical solid composition associated with InN_yAs_{1-y} as a function of inlet NH_3 gas concentration. By applying Eq. (11) to this system, it is expected that N incorporation into InAs may be as low as $y<1.4\times10^{-5}$. However, the calculated N solid fractions are found to be within the range of theoretical solubility limits. Figure 4(c) shows that the fraction of N in the solid

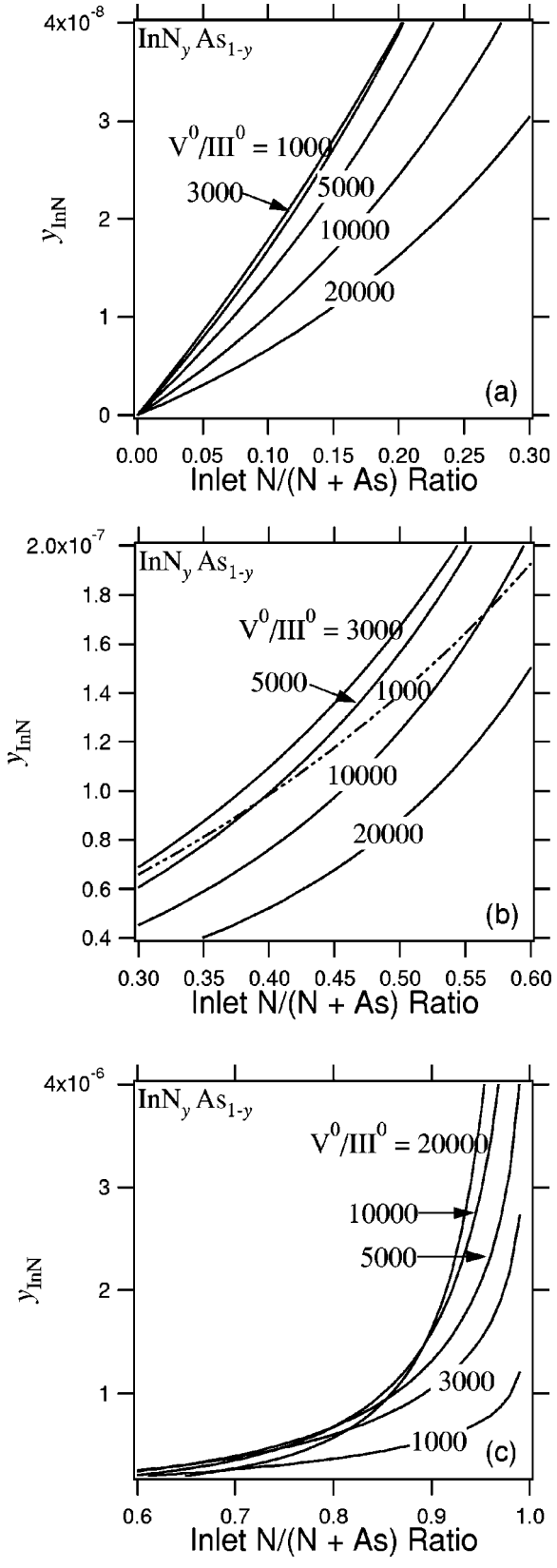

FIG. 4. Solid vs gas composition for the alloy InN_yAs_{1-y}, for $P^0_{In}=1.0\times10^{-5}$ atm, growth temperature of 700 °C, inlet V/III ratios 1000–20 000, mole fraction of NH_3 decomposing $\alpha=0.0$, and H_2 fraction $F=0.01$. The inlet N/(N+As) ratios range from (a) 0.0 to 0.3; (b) 0.3 to 0.6; and (c) 0.6 to 1.0.

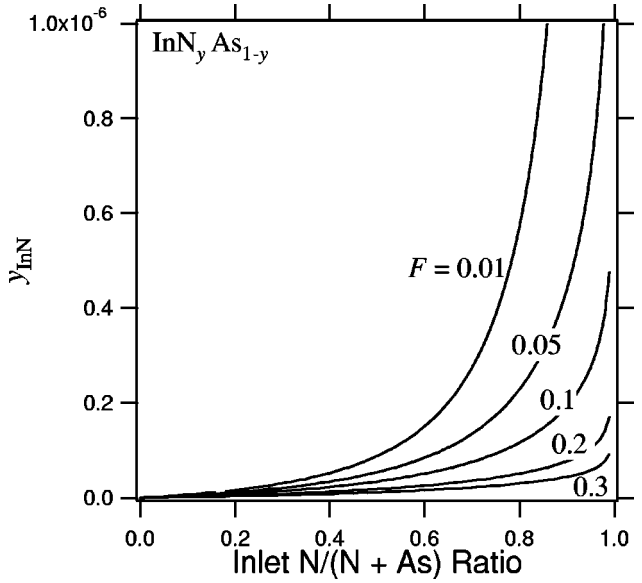

FIG. 5. Solid vs gas composition for the alloy InN_yAs_{1-y}, for $P^0_{In}=1.0\times10^{-5}$ atm, growth temperature of 700 °C, $V^0/III^0=20\,000$, mole fraction of NH_3 decomposing $\alpha=0.0$, and H_2 fraction F ranging from 0.01 to 0.3.

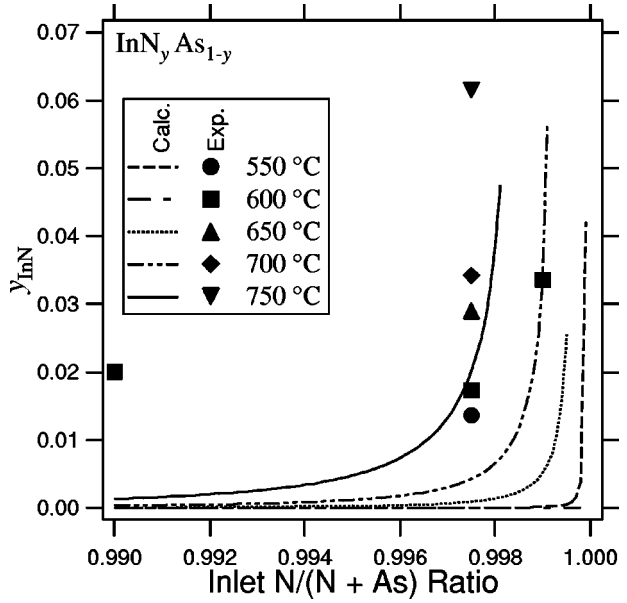

FIG. 6. Solid vs gas composition for the alloy InN_yAs_{1-y}, for $P^0_{In}=1.8\times10^{-6}$ atm, growth temperatures ranging from 550 to 750 °C, $V^0/III^0=50\,000$, mole fraction of NH_3 decomposing $\alpha=0.0$, and H_2 fraction $F=0.0$. The experimental data are from Ref. 35.

increases with increasing V^0/III^0 at higher $P^0_{NH_3}$, while the solid composition of N decreases with increasing inlet V/III ratios at lower $P^0_{NH_3}$, as seen in Fig. 4(a). The preferential incorporation of As over N is observed at low $P^0_{NH_3}$, and this can be explained by the limited solubility of N into this alloy. While the trends for N incorporation are monotonic at low and high $P^0_{NH_3}$, as seen in Fig. 4(b) the dependence is more complicated at intermediate gas-phase concentrations $(0.3<P^0_{NH_3}/P^0_V<0.6)$. The solid composition of N increases with increasing inlet V/III ratio until $V^0/III^0\approx3000$, and then it decreases with further increases in this ratio. Figure 5 illustrates the effect of H_2 mole fraction in the carrier gas. In Fig. 5, unlike the varying dependence of N solid composition on $P^0_{NH_3}$ found in Fig. 4, it is observed that the solid composition of N monotonically increases with decreasing the value of the parameter F over the entire range of gas-phase N compositions. The N solid fraction is significantly larger when the H_2 fraction in the carrier gas is reduced to 1%. A comparison between the predicted solid composition and experimental data[35] is shown in Fig. 6. The calculated values of N solid fraction are all lower than the corresponding experimental values. At lower processing temperatures, from 550 to 650 °C, the N solid fraction remains very low, on the order of 10^{-5}, until the $P^0_{NH_3}/P^0_V$ ratio approaches unity. For values of $P^0_{NH_3}/P^0_V>0.995$, the N solid fraction depends strongly on this ratio. Thus, any errors in the measurement of $P^0_{NH_3}$ or $P^0_{AsH_3}$ will greatly magnify the apparent discrepancy between the calculated and experimental solid compositions.

AlN_yAs_{1-y}: Figure 7 shows the predicted solid composition of AlN_yAs_{1-y} as a function of $P^0_{NH_3}$. The calculated N solid compositions shown in Fig. 7 are far greater than the theoretical solubility limit, calculated to be $O(10^{-12})$, indicating that the thermodynamic chemical equilibrium model that results in Eq. (11) may not be not realistic for this nitride alloy. Figure 7 demonstrates that the N solid composition increases with increasing $P^0_{NH_3}$, but the dependence of solid composition on inlet V/III ratio is not monotonic. For example, at higher $P^0_{NH_3}$ the values of y_{AlN} for $V^0/III^0=5$ exceed those for $V^0/III^0=10$. Additional calculations demonstrate that the solid fraction of N in this alloy increases as the fraction of H_2 in the carrier gas is decreased; the solid composition of N is increased significantly when the H_2 mole fraction in the inert carrier gas is reduced to 1%.

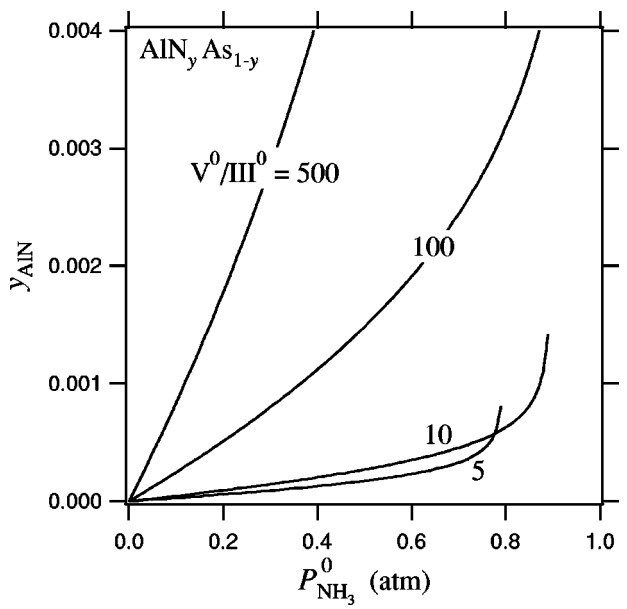

FIG. 7. Solid vs gas composition for the alloy AlN_yAs_{1-y}, for $P^0_{Al}=1.0\times10^{-5}$ atm, growth temperature of 700 °C, inlet V/III ratios 5–500, mole fraction of NH_3 decomposing $\alpha=0.0$, and H_2 mole fraction $F=1.0$.

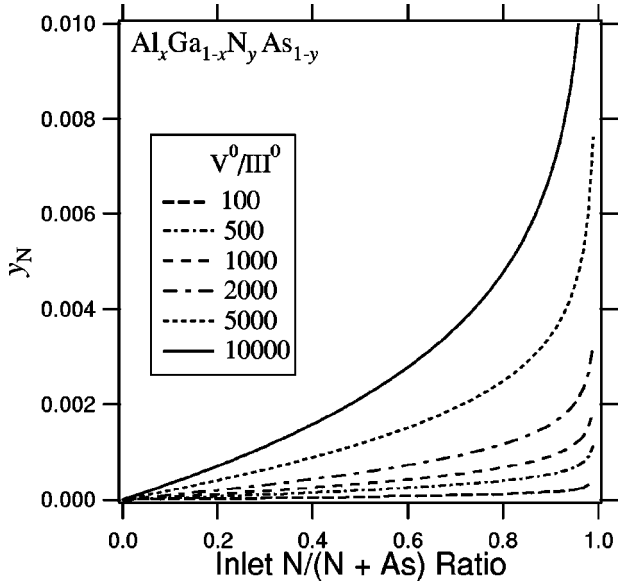

FIG. 8. Solid vs gas composition for the alloy $Al_xGa_{1-x}N_yAs_{1-y}$, for $P^0_{III}=1.0\times10^{-5}$ atm, $P^0_{TMAl}/P^0_{III}=0.5$, growth temperature of 700 °C, inlet V/III ratios 100–10 000, mole fraction of NH_3 decomposing $\alpha=0.0$, and H_2 mole fraction $F=1.0$.

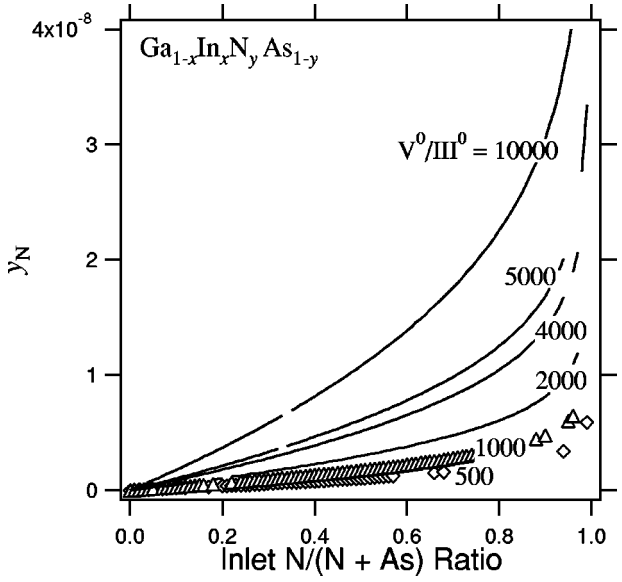

FIG. 10. Solid vs gas composition for the alloy $Ga_{1-x}In_xN_yAs_{1-y}$, for $P^0_{III}=1.0\times10^{-5}$ atm, $P^0_{TMIn}/P^0_{III}=0.5$, inlet V/III ratios 500–10 000, mole fraction of NH_3 decomposing $\alpha=0.0$, and H_2 mole fraction $F=1.0$.

3. Quaternary III–III–N–V alloys

Figures 8–13 show the predicted solid–gas compositions of the quaternary nitrides $Al_xGa_{1-x}N_yAs_{1-y}$, $Al_xIn_{1-x}N_yAs_{1-y}$, and $Ga_xIn_{1-x}N_yAs_{1-y}$. These materials show promise for use in a number of applications, such as multijunction tandem solar cells in the case of $Ga_xIn_{1-x}N_yAs_{1-y}$. A solar cell with a 1.0 eV band gap and internal quantum efficiency greater than 70% has been developed using this alloy.[33] It is predicted that the solid composition of N monotonically increases with increasing $P^0_{NH_3}$, as shown in Figs. 8–10. Unlike the ternary III–N–As system, N solid composition in the quaternary alloy increases monotonically with increasing inlet V/III ratios. It is also observed that the solid composition of N monotonically increases with decreasing F over the entire range of N gas-phase concentrations, as illustrated in Figs. 11–13. As with the ternary nitride compounds, the presence of H_2 in the carrier gas has a significant effect on N solid composition.

4. Quaternary III–N–V–V alloy

$AlN_xP_yAs_{1-x-y}$: Figures 14 and 15 show the theoretical predictions of solid composition for $AlN_xP_yAs_{1-x-y}$ as a

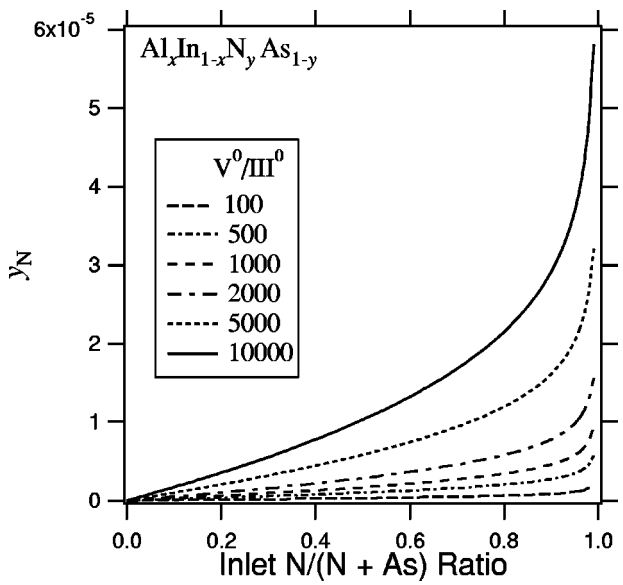

FIG. 9. Solid vs gas composition for the alloy $Al_xIn_{1-x}N_yAs_{1-y}$, for $P^0_{III}=1.0\times10^{-5}$ atm, $P^0_{TMAl}/P^0_{III}=0.5$, inlet V/IIII ratios 100–10 000, mole fraction of NH_3 decomposing $\alpha=0.0$, and H_2 mole fraction $F=1.0$.

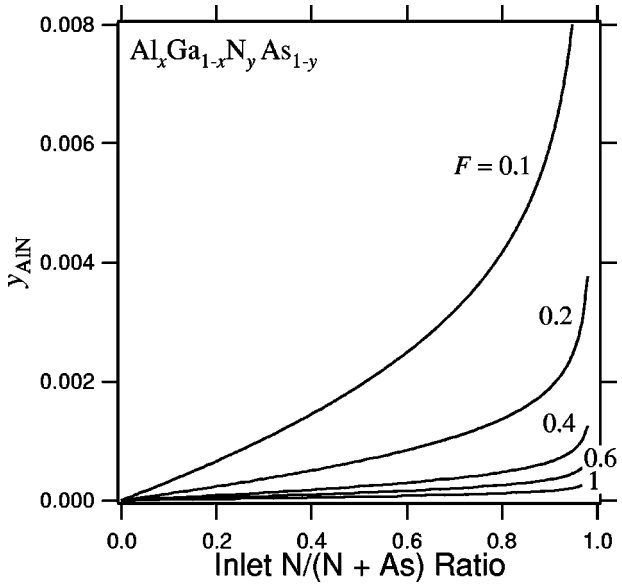

FIG. 11. Solid vs gas composition for the alloy $Al_xGa_{1-x}N_yAs_{1-y}$, for $P^0_{III}=1.0\times10^{-5}$ atm, $P^0_{TMAl}/P^0_{III}=0.5$, growth temperature of 700 °C, $V^0/III^0=100$, mole fraction of NH_3 decomposing $\alpha=0.0$, and H_2 mole fraction F ranging from 0.1 to 1.0.

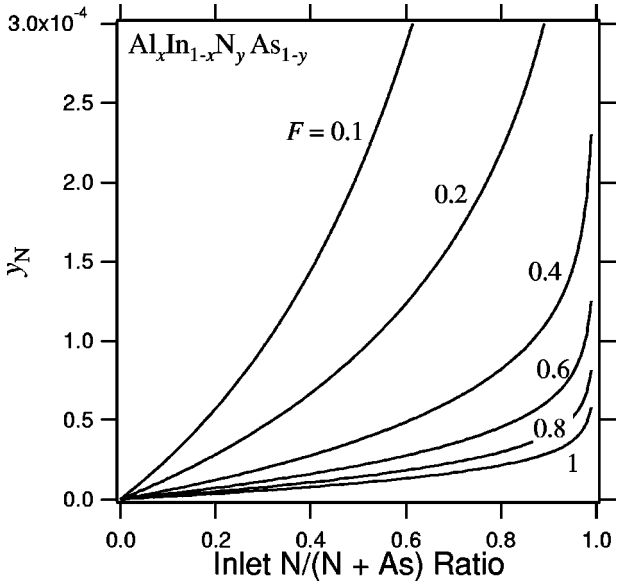

FIG. 12. Solid vs gas composition for the alloy $Al_xIn_{1-x}N_yAs_{1-y}$, for $P^0_{III}=1.0\times10^{-5}$ atm, $P^0_{TMAl}/P^0_{III}=0.5$, $V^0/III^0=10\,000$, mole fraction of N H_3 decomposing $\alpha=0.0$, and H_2 mole fraction F ranging from 0.1 to 1.0.

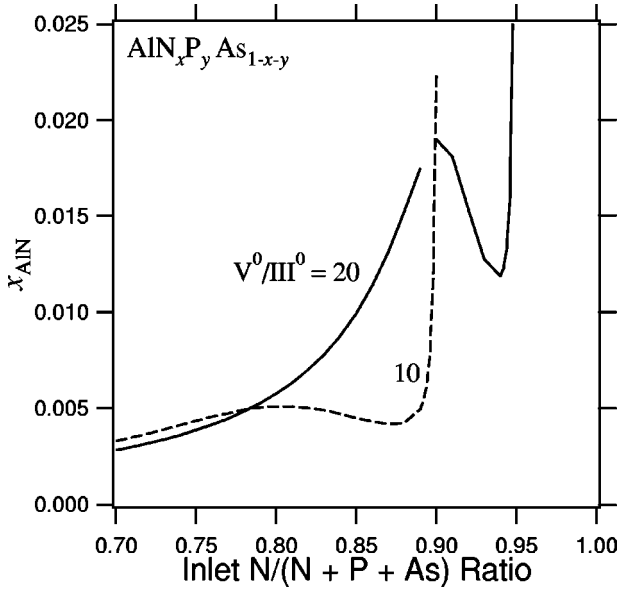

FIG. 14. Solid vs gas composition for the alloy $AlN_xP_yAs_{1-x-y}$, for $P^0_{Al}=1.0\times10^{-5}$ atm, $P^0_{NH_3}/P^0_{PH_3}=1$, growth temperature of 600 °C, V^0/III^0 ratios=10 and 20, mole fraction of NH_3 decomposing $\alpha=0.0$, and H_2 mole fraction $F=1.0$.

function of inlet NH_3 fraction. As in previous calculations, the equilibrium constants associated with AlP and AlAs deposition are obtained from Koukitu *et al.*[20,21] Figure 14 shows that the solid composition of N for $V^0/III^0=10$ and 20. The calculated N solid compositions in this figure are much higher than the estimated N solubility limit in both the AlP alloy (1.3×10^{-9}) and AlAs alloy (1.0×10^{-12}). Therefore, the predicted compositions in Fig. 14 may have no physical significance, or more likely, these results may indicate that the model is not appropriate for calculating the N solubility limit for this alloy, as was pointed out by Schilfgaarde *et al.*[25] However, the interesting feature in this figure is that the curves have local maximum and minimum points. This behavior may be due to the nonideality in the solid phase at higher solid N concentrations. Figure 15 indicates that the N solid composition increases with decreasing H_2 fraction in the carrier gas. Most of the solid compositions of N in this figure are, again, much higher than the estimated N solubility limit both in AlP and AlAs, and this may be due to nonideality in the solid at higher solid composition of N. Although the curves for higher values of F display no ex-

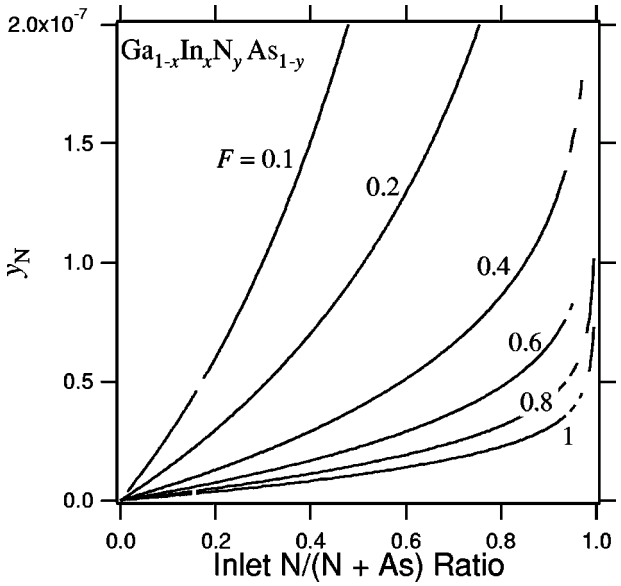

FIG. 13. Solid vs gas composition for the alloy $Ga_{1-x}In_xN_yAs_{1-y}$, for $P^0_{III}=1.0\times10^{-5}$ atm, $P^0_{TMIn}/P^0_{III}=0.5$, $V^0/III^0=10\,000$, mole fraction of N H_3 decomposing $\alpha=0.0$, and H_2 mole fraction F ranging from 0.1 to 1.0.

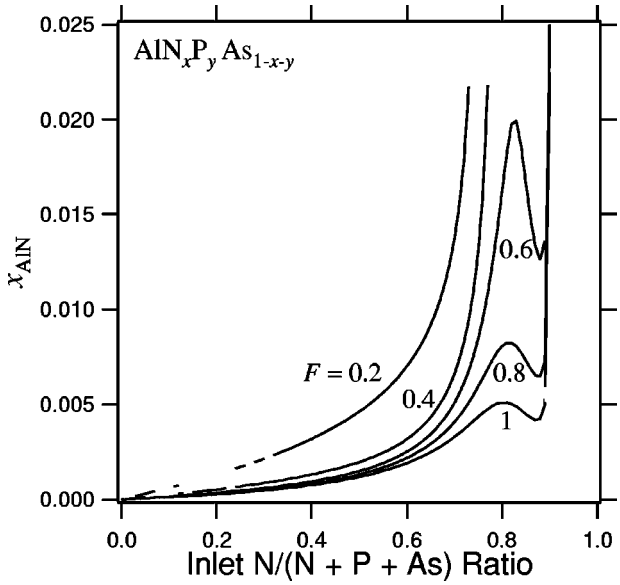

FIG. 15. Solid vs gas composition for the alloy $AlN_xP_yAs_{1-x-y}$, for $P^0_{Al}=1.0\times10^{-5}$ atm, $P^0_{NH_3}/P^0_{PH_3}=1$, growth temperature of 600 °C, $V^0/III^0=10$, mole fraction of NH_3 decomposing $\alpha=0.0$, and H_2 mole fraction F ranging from 0.2 to 1.0.

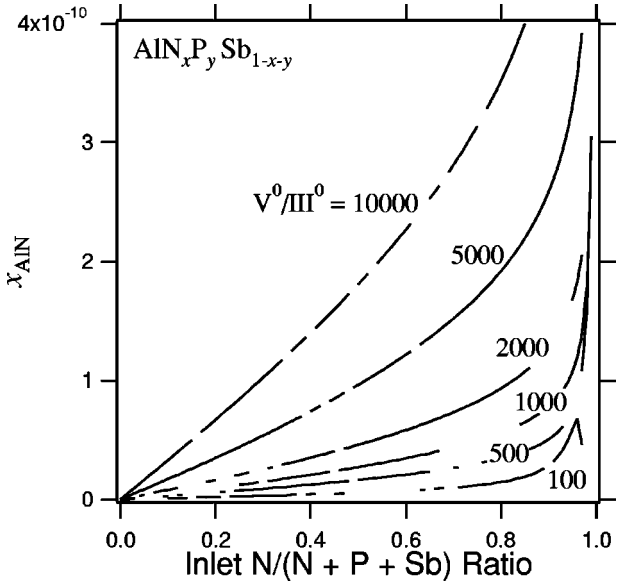

FIG. 16. Solid vs gas composition for the alloy $AlN_xP_ySb_{1-x-y}$, for $P^0_{Al} = 1.0\times10^{-5}$ atm, $P^0_{PH_3}/P^0_{TMSb} = 1$, growth temperature of 600 °C, inlet V/III ratios 100–10 000, mole fraction of NH_3 decomposing $\alpha = 0.0$, and H_2 mole fraction $F = 1.0$.

trema, they may have local maximum and minimum points at higher solid compositions of N ($x > 0.2$) where numerical solutions could not be obtained.

$AlN_xP_ySb_{1-x-y}$: Figures 16 and 17 contain the theoretical results for N solid composition in $AlN_xP_ySb_{1-x-y}$ as a function of $P^0_{NH_3}$. Although the solid compositions of N in Fig. 16 are all below the N solubility limit in the AlP alloy, 1.3×10^{-9}, some of these values are larger than the exceptionally low estimate for the solubility limit of N in the AlSb alloy, 4.7×10^{-19}. Again, this result indicates that, either the present model fails to predict solid composition due to nonideal solid solution behavior, or Eq. (11) is not quantitative due to the failure of this model when applied to nitrides. Regardless, several features present in these results may account for important aspects observed in the III–V nitride system. First, the N solid compositions calculated for $AlN_xP_ySb_{1-x-y}$ are smaller than those calculated for AlN_yP_{1-y}, indicating that the incorporation of nitrogen into quaternary alloys is more difficult than into ternary alloys. Second, the curve for inlet V/III ratio of 100 has a local maximum point. Finally, Fig. 17 correctly demonstrates that the N solid composition increases with decreasing the fraction of H_2 in the carrier gas.

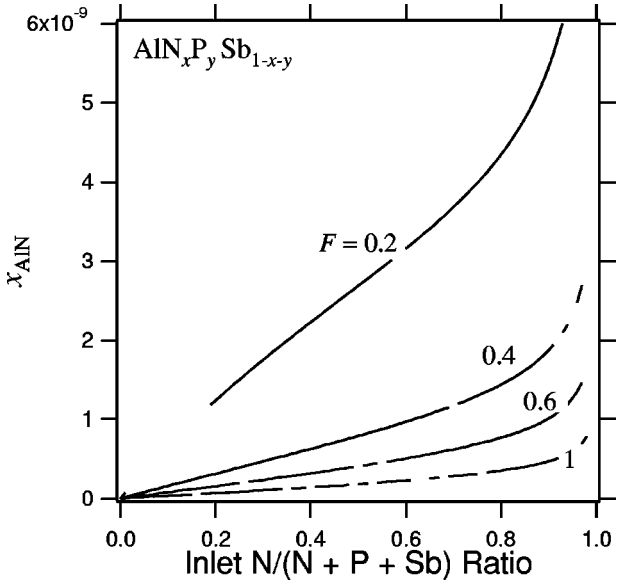

FIG. 17. Solid vs gas composition for the alloy $AlN_xP_ySb_{1-x-y}$, for $P^0_{Al} = 1.0\times10^{-5}$ atm, $P^0_{PH_3}/P^0_{TMSb} = 1$, growth temperature of 600 °C, $V^0/III^0 = 10\,000$, mole fraction of NH_3 decomposing $\alpha = 0.0$, and H_2 mole fraction F ranging from 0.08 to 0.4.

IV. CONCLUSION

A thermodynamic analysis for non-nitride III–V semiconductor alloys grown by MOVPE has been applied to systematically study these materials. The solid composition has been calculated for ternary and quaternary alloys as a function of inlet gas concentration, and the predicted solid compositions have been compared with available experimental data. For alloys that do not contain phosphorus, good agreement is seen when no adjustable parameters are used in the model, indicating that the solid composition of these alloys is thermodynamically controlled; in such systems chemical equilibrium is clearly established at the gas–solid interface. For P-containing alloys, an extended quasithermodynamic equilibrium model has been applied. Introduction of one adjustable parameter, f, representing kinetically limited PH_3 decomposition, has resulted in reasonable agreement between calculated and experimental compositions for InP_yAs_{1-y}. Due to the incomplete pyrolysis of PH_3, the Gibbs free energy of formation of component binary compounds alone cannot determine the solid composition of these alloys in MOVPE.

It has been observed in this work that the inlet concentrations of the group III metalorganic sources strongly influence the incorporation of P into the solid for the quaternary III–III–P–As system. However, the inlet mole fraction of the group V hydride sources has no influence on the incorporation of the group III elements into the solid. This difference may account for the fact that III–V semiconductor growth by MOVPE is mass transport limited with respect to group III molecules.

A thermodynamic analysis for nitride III–V semiconductor alloys grown by MOVPE has also been carried out to predict the behavior of these systems. The calculation procedure is similar to that for non-nitride alloys, but two parameters have been introduced—α and F—where α is the mole fraction of NH_3 that decomposes and F is the H_2 mole fraction in the inert carrier gas. The resulting solid composition depends strongly on the inlet V/III ratio, such that the solid fraction of N increases monotonically with increasing V^0/III^0 for quaternary nitrides. However, this monotonic trend is not predicted for ternary alloys such as InN_yAs_{1-y}. Among the quaternary nitrides, the apparent mechanism of N incorporation into the solid is the most complicated for the

III–N–V–V system. It is predicted here that, for these quaternary alloys, the fraction of N in the solid is not always monotonic with $P^0_{NH_3}/P^0_V$, such that the actual functionality depends in a nonlinear manner on V^0/III^0 and F. This behavior has also been observed by Naoi *et al.*,[35] but further investigation is necessary to explain these observations. For both ternary and quaternary alloys, larger input V/III ratios ($V^0/III^0 > 1000$) and $P^0_{NH_3}/P^0_V > 0.9$ are often required to obtain sufficient N solid composition. However, the N solid fraction is smaller in quaternary (III–N–V–V) alloys than in ternary alloys, indicating that the interaction parameter or enthalpy of mixing is larger for these types of alloys. The present thermodynamic equilibrium model tends to predict N solid compositions greater than the theoretical solubility limit, particularly for Al-containing ternary nitrides. This may be attributed either to a shortcoming in the present model when calculating N solid compositions or to a failure of Eq. (11) because of inadequacies in the VFF model when applied to nitrides. However, the present model does predict N solid compositions smaller than the solubility limit for In-containing ternary and quaternary nitrides. Thus, insofar as In-containing nitrides are concerned, the calculated results of N solid composition are believed to be reliable.

The role of H_2 in nitride systems has been investigated for various ternary and quaternary nitrides. It is shown that the solid composition of N increases with parameter F decreased. In other words, the solid composition of N significantly increases when the partial pressure of H_2 in the carrier gas is decreased. The reactions leading to nitride deposition proceed more effectively in the inert gas system, and these reactions are suppressed when H_2 concentration is increased. Therefore, in the case of nitride alloys, it is important to use an inert carrier gas to obtain higher N solid concentrations.

ACKNOWLEDGMENTS

This work has been supported by the Gas/Surface Dynamics Section of the Naval Research Laboratory, Contract No. N00014-97-1-G020. The authors would like to thank Dr. M. Coltrin for his assistance in evaluating the model.

[1] G. B. Stringfellow, J. Cryst. Growth **62**, 225 (1985).
[2] G. B. Stringfellow and M. J. Cherng, J. Cryst. Growth **64**, 413 (1984).
[3] G. B. Stringfellow, J. Cryst. Growth **68**, 111 (1984).
[4] G. B. Stringfellow and M. J. Cherng, J. Cryst. Growth **70**, 133 (1984).
[5] M. J. Cherng, R. M. Cohen, and G. B. Stringfellow, J. Electron. Mater. **13**, 799 (1984).
[6] M. J. Jou and G. B. Stringfellow, J. Cryst. Growth **98**, 679 (1989).
[7] H. Seki and A. Koukitu, J. Cryst. Growth **74**, 172 (1986).
[8] A. Koukitu and H. Seki, J. Cryst. Growth **76**, 233 (1986).
[9] S. Nakamura, T. Mukai, and M. Senoh, Appl. Phys. Lett. **64**, 1687 (1994).
[10] S. Nakamura, M. Senoh, N. Isawa, S. Nagahama, T. Yamada, and T. Mukai, Jpn. J. Appl. Phys., Part 2 **34**, L1332 (1995).
[11] S. Nakamura, M. Senoh, S. Nagahama, N. Isawa, T. Yamada, T. Matsushita, Y. Sugimoto, and H. Kiyoku, Appl. Phys. Lett. **69**, 3034 (1996).
[12] R. P. Schneider, Jr. and J. A. Lott, Appl. Phys. Lett. **63**, 917 (1993).
[13] K. Tai, L. Yang, Y. H. Wang, J. D. Wynn, and A. Y. Cho, Appl. Phys. Lett. **56**, 2496 (1990).
[14] A. Koukitu, N. Takahashi, T. Taki, and H. Seki, Jpn. J. Appl. Phys., Part 2 **35**, L673 (1996).
[15] A. Koukitu and H. Seki, Jpn. J. Appl. Phys., Part 2 **35**, L1638 (1996).
[16] A. Koukitu, N. Takahashi, and H. Seki, Jpn. J. Appl. Phys., Part 2 **36**, L1136 (1997).
[17] A. Koukitu, N. Takahashi, T. Taki, and H. Seki, J. Cryst. Growth **170**, 306 (1997).
[18] G. B. Stringfellow, J. Electrochem. Soc. **119**, 1780 (1972).
[19] B. G. Stringfellow, J. Cryst. Growth **27**, 21 (1974).
[20] A. Koukitu and H. Seki, Jpn. J. Appl. Phys., Part 1 **21**, 1675 (1982).
[21] H. Seki and A. Koukitu, Record Second III–V Alloy Semiconductor Physics and Electronic Seminar, Hamamatsu, March 1983, p. 19.
[22] L. B. Pankratz, Thermodynamic Properties of Elements and Oxides, United States Department of the Interior Bureau of Mines, 1982.
[23] I.-H. Ho and G. B. Stringfellow, J. Cryst. Growth **178**, 1 (1997).
[24] P. N. Keating, Phys. Rev. **145**, 637 (1966).
[25] M. van Schilfgaarde, A. Sher, and A.-B. Chen, J. Cryst. Growth **178**, 8 (1997).
[26] G. B. Stringfellow, *Organometallic Vapor-Phase Epitaxy: Theory and Practice* (Academic, New York, 1989), p. 27.
[27] C. A. Larsen and G. B. Stringfellow, J. Cryst. Growth **75**, 247 (1986).
[28] C. A. Larsen, N. I. Buchan, and G. B. Stringfellow, J. Cryst. Growth **85**, 148 (1987).
[29] T. Fukui and Y. Horikoshi, Jpn. J. Appl. Phys., Part 1 **20**, 587 (1981).
[30] M. J. Ludowise and W. T. Dietze, J. Electron. Mater. **11**, 59 (1982).
[31] S. Keller, B. P. Keller, D. Kapolnek, and A. C. Abare, Appl. Phys. Lett. **68**, 3147 (1996).
[32] V. Härle, H. Bolay, F. Steuber, F. Scholz, V. Syganow, G. Frankowsky, and A. Hangleiter, Proceedings International Symposium on Blue Lasers and Light Emitting Diodes, Chiba, Japan, 1996, p. 62.
[33] S. R. Kurtz, A. A. Allerman, E. D. Jones, J. M. Gee, J. J. Banas, and B. E. Hammons, Appl. Phys. Lett. **74**, 729 (1999).
[34] T. Matsuoka, N. Yoshimoto, T. Sakai, and A. Katsui, J. Electron. Mater. **21**, 157 (1992).
[35] H. Naoi, Y. Naoi, and S. Sasaki, Solid-State Electron. **41**, 319 (1997).